An Interference Alignment and ICA Based Semi-Blind Dual-User Downlink NOMA System for High-Reliability Low-Latency IoT

Xin Wan, Xu Zhu, *Senior Member, IEEE*,Yufei Jiang, *Member, IEEE*,
Yujie Liu, *Student Member, IEEE* and Jiahe Zhao .

***Abstract*—An interference alignment (IA) and independent component analysis (ICA) based semi-blind scheme, referred to as IA-ICA, is proposed for downlink dual-user power-domain non-orthogonal multiple access (NOMA) systems in high-reliability low-latency (HRLL) Internet of Things (IoT). At base station (BS), one user is converted to constructive interference to the other user via phase alignment of each symbol. At both user ends, ICA is used for semi-blind signal detection. The phase rotation via non-redundant precoding at BS does not introduce any spectral overhead, while only 1-2 pilot symbols are required for elimination of ICA incurred ambiguity. Closed-form expressions are derived for the users' symbol error rate (SER) performance in Rayleigh fading with 4-quadrature amplitude modulation (4-QAM), which match the simulation results very well. Based on the analytical results, we propose an efficient power allocation algorithm that is based on statistical channel state information (CSI) only, and therefore the signaling overhead involved is negligible. In particular, a near-optimal SER performance can be achieved with equal power allocation between the two users. The proposed IA-ICA based semi-blind NOMA system demonstrates a much better SER performance than the existing approaches even though they are under perfect CSI. Hence, it is a feasible solution for HRLL IoT, with high reliability and very low spectral and signaling overheads.**

***Index Terms*—Non-orthogonal multiple access (NOMA), high-reliability low-latency (HRLL) Internet of Things (IoT), interference alignment (IA), independent component analysis (ICA).**

I. Introduction

INTERNET of things (IoT) [1] has become one of the most important sectors in the technology field. Many real-time IoT scenarios have stringent requirements on reliability and latency, such as autonomous driving, remote medical care and industrial applications [2] [3] that may not be met by existing networks. The fifth generation (5G) wireless communications is the enabler of high-reliability and low-latency (HRLL) IoT with a massive number of devices connected [4] [5]. Meanwhile, it is usually challenging to maintain high reliability and low latency at the same time with restricted bandwidth [5] [6].

Non-orthogonal multiple access (NOMA) [7], which allows multiple users to share the same frequency or code resources simultaneously [8], is regarded as a promising technique to support massive connectivity and handle the challenges of resource collisions thus reduce latency [9]–[12]. NOMA has been proved to have enhanced spectrum efficiency (SE), lower system delay and higher user fairness than orthogonal multiple access (OMA) [13]. Power-domain NOMA [13] is one of the most widely investigated NOMA schemes, where different users are multiplexed in power domain and their signals are superimposed at base station (BS) in the downlink.

A. Related Work

Most existing work on power-domain NOMA has focused on studying the energy efficiency (EE), outage probability, or user fairness [14]–[17]. An iterative user scheduling and power allocation algorithm was proposed in [14] to maximize the EE of NOMA systems with imperfect channel state information (CSI). The outage probabilities and ergodic rates of a NOMA system were derived in [15]. In [16], a multiple-input multiple-output (MIMO) NOMA relaying system was investigated, where the sum rate and outage probability were optimized by antenna selection and power allocation, respectively. A joint user pairing and power allocation algorithm was proposed for an uplink NOMA cellular network in [17] towards proportional fairness of users. In [18], the transmission rate of a dual-user power-domain NOMA system in a short-packet regime was optimized. All the aforementioned work has assumed that there is a channel gain disparity between the users in a NOMA pair and that the CSI is known perfectly at BS.

It is challenging to maintain high reliability of NOMA due to inter-user interference [19] [20]. Successive interference cancellation (SIC) [21] is a widely used detection scheme for downlink power-domain NOMA, which separates the signals of different users by their power differences. Specifically, the signal transmitted to the user with weaker channel condition is allocated more power and decoded with a higher order at the receiver, and their contribution to the received signal is canceled at each layer of detection. However, SIC incurs error propagation [22] across users, and suffers an error floor when the users are allocated a similar amount of transmission power. Therefore, SIC is not applicable to NOMA for HRLL IoT.

Manuscript received November 20, 2019; revised March 9, 2020 and March 25, 2020; accepted April 18, 2020. *(Corresponding author: Xu Zhu, Yufei Jiang.)*

X. Wan, Y. Jiang and J. Zhao are with the School of Electronic and Information Engineering, Harbin Institute of Technology, Shenzhen 518055, China (e-mail: 18s052112@stu.hit.edu.cn, Jiangyufei@hit.edu.cn and 18s052119@stu.hit.edu.cn).

X. Zhu and Y. Liu are with the Department of Electrical and Electronics Engineering, University of Liverpool, Liverpool L69 3GJ, U.K. Y. Liu is also with the Department of Electrical and Electronic Engineering, Xi'an Jiaotong-Liverpool University, Suzhou 215123, China (e-mail: xuzhu@liverpool.ac.uk and yujieliu@liverpool.ac.uk)

An interference dissolution scheme was proposed in [23] to address the error floor issue of SIC in a dual-user NOMA system with equal power allocation. Whereas, it requires high complexity and a strict assumption of equal path losses (PLs) at the two users. In [24] and [25], constellation rotation was employed to enhance the reliability of NOMA. However, the work in [24] was restricted to additive white Gaussian noise (AWGN) channel, and the optimal rotation angle and the resulting error performance are highly dependent on power allocation. In [25], joint optimization of power allocation and modulation was conducted at the transmitter and maximum likelihood detection (MLD) was conducted at the receivers, assuming perfect CSI at the transmitter. MLD is an optimal nonlinear detection scheme that estimates symbols by maximizing a likelihood function, and its complexity increases exponentially with symbols and the order of modulation. The rotation angle in [25] was chosen by maximizing the smallest Euclidean distance in error pairs and applied to only one user in a pair. However, its dynamic power allocation strategy requires excessive signaling overhead, which prevents its application in HRLL IoT.

There also lacks error probability analysis of NOMA in the literature. In [26] and [27], the analytical bit error rate (BER) of power-domain NOMA with SIC was derived. However, their channels were assumed to be AWGN channel. In [28], NOMA was combined with generalized space shift keying (GSSK) in a MIMO system to improve both SE and error performance. However, it assumed perfect SIC which is unrealistic and BER results of only cell-edge user were presented.

All the aforementioned work is under the assumption of perfect CSI, which however is hard to obtain in practice [29]. The estimation of CSI and feedback of CSI to BS is a crucial issue, especially for HRLL IoT. It is particularly important to reduce the signaling and spectral overhead involved in short-packet transmission while maintaining high reliability. The impact of pilot overheads on various system parameters such as packet size and error probability was investigated and optimized in [30] for a point-to-point communication. Data symbols were used as virtual pilots in [31] to improve the accuracy of channel estimation in short-packet transmission.

Independent component analysis (ICA) [32] is an effective blind source separation approach that separates independent non-Gaussian source signals based on the higher order statistics of their linear mixtures. In [33], ICA was employed for channel estimation in a MIMO system and achieves a performance close to the case with perfect CSI with only few pilots. To avoid pilot contamination in a multiuser massive MIMO uplink system, a semi-blind decoding scheme based on ICA and reference bits was proposed in [34]. ICA is more spectrum efficient than the conventional detection approaches for downlink NOMA since training for channel estimation and CSI feedback is not required. To the best of our knowledge, ICA has not been applied to in NOMA systems.

B. Contributions

In this paper, an interference alignment (IA) and ICA (IA-ICA) based semi-blind dual-user downlink NOMA system is proposed for HRLL IoT. The two users are simply classified as far user (FU) and near user (NU) by their distance to BS. At BS, IA is implemented by rotating the phase of NU's symbol to align with that of FU's symbol so that NU becomes constructive interference to FU. At both user ends, ICA rather than SIC is applied to recover the data in a semi-blind manner. Our contributions are as follows.

- To the best of our knowledge, this is the first work to introduce a semi-blind structure to NOMA systems for HRLL IoT, which provides highly reliable signal detection at very low spectral overhead. IA improves the signal-to-interference-plus-noise-ratio (SINR) significantly via phase rotation. The purpose of phase rotation is different from that in [24] and [25], where it used to increase the minimum distance between the superimposed constellation points with limited performance enhancement. The phase rotation information is carried by a non-redundant precoding, introducing no spectral overhead. The only spectral overhead required by the semi-blind IA-ICA structure involves only 1-2 pilot symbols that are used for elimination of ambiguities caused by ICA. The proposed semi-blind IA-ICA structure achieves a much better symbol error rate (SER) performance than the SIC based approach [21] and other phase rotation based approaches [24] [25] for NOMA, even though they are under perfect CSI. Its performance is also robust against frame length even if the frame length is less than 100, demonstrating its feasibility for low latency communications.
- With the proposed IA-ICA scheme, closed-form expressions are derived for FU's SER and the upper bound on NU's SER as well as their asymptotic forms in Rayleigh fading, with 4-quadratrure amplitude modulation (4-QAM) applied. The analytical results, as a function of the precoding constant and the power allocation coefficient, match the simulation results very well. While the previous analyses on error probability of NOMA [26] [27] were dedicated to SIC based NOMA systems and restricted to AWGN channel.
- We propose a statistical CSI based inter-user and intra-user power allocation algorithm to minimize the average asymptotic SER derived. This is the first power allocation strategy for NOMA that depends on statistical CSI (PL ratio) only and does not require a channel gain disparity of the users, resulting in negligible signaling overhead and much lower computational complexity, compared to the previous power allocation approaches that are based on instantaneous CSI estimated and fed back to BS [21] [25]. In particular, a near-optimal SER performance can be achieved with equal power allocation between the two users. Thus, a two-dimensional (2D) power allocation problem reduces to a low-complexity one-dimensional (1D) searching problem aimed to find the optimal precoding coefficient for intra-user power allocation between NU's source symbol and a superimposed reference data in precoding.
- The IA-ICA scheme enables higher physical layer secu-

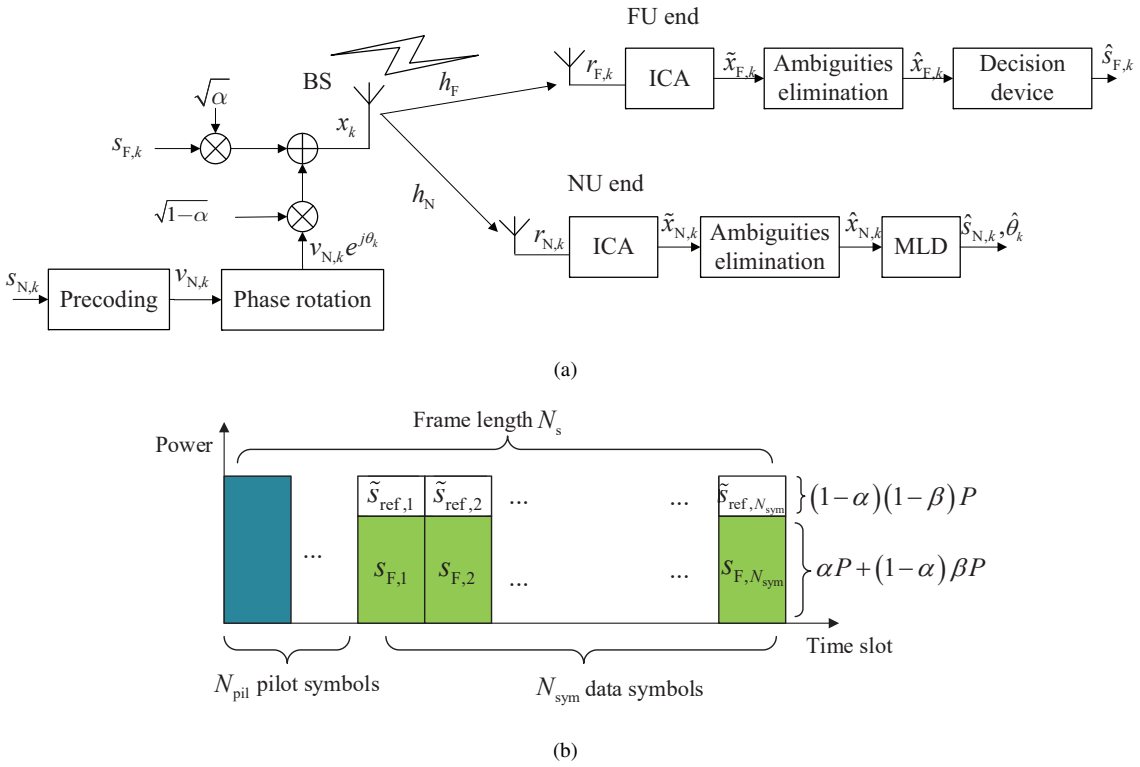

Fig. 1. (a) Block diagram of IA-ICA scheme, (b) frame structure of the superimposed data x_k. (N_{pil}: number of pilot symbols in a frame, N_{sym}: number of data symbols in a frame.)

rity. In the previous work with SIC [16] [21], FU could act as a potential eavesdropper and decode the entrusted NU's data [35] [36]. While with the proposed IA-ICA scheme, FU cannot track the correct phase rotation to decode NU's data, thanks to NU's reference data in non-redundant precoding which is unknown to FU.

C. Organization and Notations

The rest of the paper is organized as follows. Section II describes the system model. The proposed IA-ICA scheme is described in Setion III. Performance analysis and the proposed power allocation algorithm are presented in Section IV. Complexity analysis is provided in Section V. Simulation results are shown in Section VI and the conclusion is drawn in Section VII.

Throughout the paper, scalars are represented by italic symbols. $(\cdot)^*$ denotes a complex conjugate, $\Re e\,(\cdot)$ denotes the real part of a complex-valued signal. $\arg\max(\cdot)$, $\mathrm{E}[\cdot]$ and $|\cdot|$ denote the points for which the maximum value is attained, the expectation operation and the absolute value of a complex-valued signal, respectively. $p\,(\cdot)$ denotes the probability of an event. Let subscripts F and N indicate FU and NU, respectively.

II. System Model

In this paper, we consider a widely used dual-user NOMA system in the downlink, where the BS and both users are equipped with a single antenna [23] [24], and 4-QAM constellation is employed. Assume that the total power allocated to the two users is P. Define N_{s} as the length of a data frame, including N_{pil} pilot symbols (for ambiguities elimination of ICA at user ends) and N_{sym} data symbols. Let $s_{\mathrm{F},k}$ and $s_{\mathrm{N},k}$ denote the k-th $(k = 1, 2, ..., N_{\mathrm{sym}})$ symbols of FU and NU, respectively, with $\mathrm{E}[|s_{\mathrm{F},k}|^2] = \mathrm{E}[|s_{\mathrm{N},k}|^2] = 1$. Unlike the conventional NOMA systems where the symbols of two users are superimposed on each other with power allocation, we apply a phase rotation to NU's symbols before superposition so that NU becomes a constructive interference to FU. Let θ_k denote the phase difference between $s_{\mathrm{F},k}$ and $s_{\mathrm{N},k}$, to NU's symbol, *i.e.*,

$$s_{\mathrm{F},k} = s_{\mathrm{N},k}e^{j\theta_k}. \tag{1}$$

A non-redundant precoding, detailed in Subsection III-A, is applied to NU's symbol $s_{\mathrm{N},k}$ prior to phase rotation, to allow retrieval of the rotated phase at NU end.

Define $v_{\mathrm{N},k}$ as the precoded NU's symbol. As illustrated in Fig. 1 (a), the k-th superimposed symbol is expressed as

$$x_k = \sqrt{\alpha P}s_{\mathrm{F},k} + \sqrt{(1-\alpha)P}v_{\mathrm{N},k}e^{j\theta_k}, \tag{2}$$

where $\alpha\,(0 < \alpha < 1)$ denotes the power allocation factor between FU and NU. In a special case with $v_{\mathrm{N},k} = s_{\mathrm{N},k}$, *i.e.*, no precoding is applied, the symbol of NU after phase rotation is identical to that of FU, *i.e.*, $s_{\mathrm{F},k} = s_{\mathrm{N},k}e^{j\theta_k}$, thus the k-th superimposed symbol in (2) becomes

$$x_k = \left(\sqrt{\alpha} + \sqrt{1-\alpha}\right)\sqrt{P}s_{\mathrm{F},k}, \tag{3}$$

as illustrated by Fig. 2 (b), in contrast to the superimposed symbol in conventional NOMA as shown in Fig. 2 (a). Thanks to the phase rotation of NU's symbol, it becomes constructive

interference to FU, and the signal-to-interference ratio is much larger than that in conventional NOMA system.

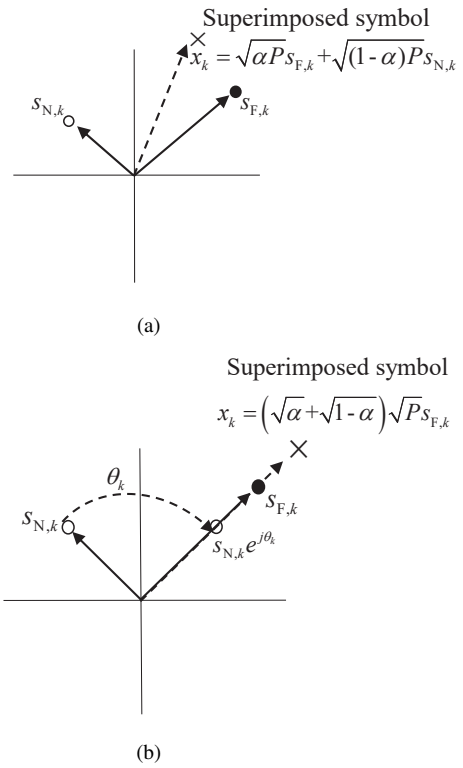

Fig. 2. Schematic diagram of the superimposed symbols in (a) the conventional NOMA system and (b) the IA-ICA based NOMA system.

We consider both large-scale and small-scale fading. Let h_{F} and h_{N} denote the channel gains of FU and NU, which are complex Gaussian random variables with a zero mean and a variance of ${\sigma_{h_{\mathrm{F}}}}^2$ and ${\sigma_{h_{\mathrm{N}}}}^2$, respectively. The received signals at FU and NU ends are respectively given by

$$r_{\mathrm{F},k} = h_{\mathrm{F}} x_k + n_{\mathrm{F},k} \tag{4}$$

and

$$r_{\mathrm{N},k} = h_{\mathrm{N}} x_k + n_{\mathrm{N},k}, \tag{5}$$

where $n_{\mathrm{F},k}$ and $n_{\mathrm{N},k}$ denote the complex-valued AWGN with zero mean and variance N_0 at FU and NU ends, respectively.

III. Semi-Blind IA-ICA Scheme

The proposed IA-ICA scheme is described in this section, whose block diagram is illustrated in Fig. 1. At BS, NU is converted to constructive interference to FU via phase rotation. A non-redundant linear precoding is applied to NU's signal prior to phase rotation, to allow retrieval of the rotated phase at NU end and also to enhance the physical layer security of NU's data. At both user ends, ICA is applied for blind signal detection, and then a series of ambiguities elimination processes are applied to recover the data by eliminating the ambiguities caused by ICA. In addition, at NU end, MLD is employed to obtain both NU's data and the rotation phase.

It is noteworthy that FU can decode its own data only, thanks to the unknown precoding and rotation information of NU, thus enabling a higher physical layer security.

If there are more than two users, phase rotation can be applied to all users to align with the farthest user, and MLD is applied at each user end except the farthest user. However, the more users, the more performance degradation will be introduced. Hence, it is preferable to assign each orthogonal resource block to two users only in NOMA systems [37] [38].

A. Precoding Aided IA

As shown in Fig. 1 (a), a non-redundant linear precoding is applied to NU's symbol $s_{\mathrm{N},k}$ prior to phase rotation, to allow retrieval of the rotated phase at NU end. The symbol after precoding is expressed as

$$v_{\mathrm{N},k} = \sqrt{\beta} s_{\mathrm{N},k} + \sqrt{1-\beta} s_{\mathrm{ref},k}, \tag{6}$$

where β $(0.5 \leq \beta \leq 1)$ denotes the precoding constant indicating the power allocation factor between NU's data and the reference data, and $s_{\mathrm{ref},k}$ is the k-th reference data designed offline. $s_{\mathrm{ref},k}$ shares the same modulation type, 4-QAM in this paper, as NU's data symbol $s_{\mathrm{N},k}$, and satisfy $\mathrm{E}[|s_{\mathrm{ref},k}|^2] = 1$, to keep the precoded signal power unchanged. It is also preferable that the phase of $s_{\mathrm{ref},k}$ aligns with that of $s_{\mathrm{N},k}$ so that it becomes constructive interference to $s_{\mathrm{N},k}$. For 4-QAM, $s_{\mathrm{N},k}$ takes four possible values with equal probability, $s_{\mathrm{ref},k}$ is randomly picked from the four symbols and kept constant at all time, achieving a maximum probability of 1/4 to be of the same phase as $s_{\mathrm{N},k}$. This also makes the signaling overhead due to precoding negligible. Therefore, in the following, we replace $s_{\mathrm{ref},k}$ by s_{ref}. Substituting (6) into (2), the superimposed signal at BS can be rewritten as

$$x_k = \sqrt{P}\left(e_1 s_{\mathrm{F},k} + e_2 \tilde{s}_{\mathrm{ref},k}\right), \tag{7}$$

where

$$e_1 = \sqrt{\alpha} + \sqrt{(1-\alpha)\beta}, \tag{8}$$

$$e_2 = \sqrt{(1-\alpha)(1-\beta)}, \tag{9}$$

and

$$\tilde{s}_{\mathrm{ref},k} = s_{\mathrm{ref}} e^{j\theta^k}, \tag{10}$$

which indicates the reference symbol with phase rotation.

The solid points $x^i\,(i = 1, \ldots, 16)$ in Fig. 3 (a) represent the composite constellation of the superimposed symbols, corresponding to x_k in (7). d_1 and d_2 represent the minimum and maximum distances from the mapping points to the origin, respectively. It can be derived that

$$d_1 = \sqrt{P/2}\left(e_1 - e_2\right), \tag{11}$$

$$d_2 = \sqrt{P/2}\left(e_1 + e_2\right). \tag{12}$$

To enable analysis of SER in the next section, the constellation in Fig. 3 (a) can be decomposed into two orthogonal mappings transmitted over the in-phase and quadrature signal components, each with half of the energy of x_k in Fig. 3 (a), as shown in Fig. 3 (b).

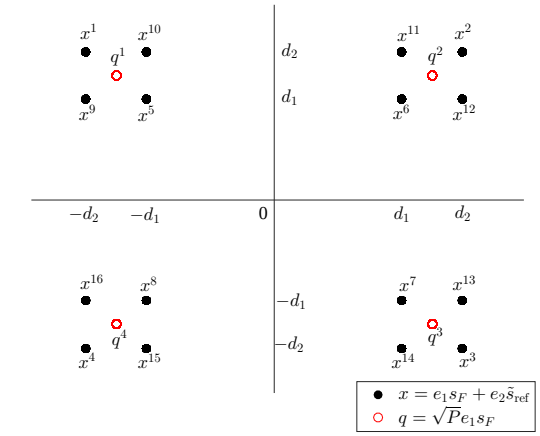

(a)

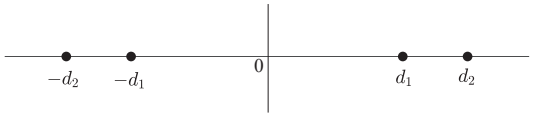

(b)

Fig. 3. (a) Composite constellation of FU's signal components and superimposed 4-QAM signals (b) Decomposition of the constellation.

B. ICA Based Signal Detection

ICA is a higher order statistics based blind signal detection approach [33], and is applied to the received signal $r_{\mathrm{F},k}$ in order to recover the transmitted signal. First, principle component analysis (PCA) [33] is applied to whiten the received signal. The whitening factor w is designed so that $|w|^2 \mathrm{E}\left[|r_{\mathrm{F},k}|^2\right] = 1$. JADE [39], a fourth order cumulants based ICA algorithm, is applied to detect the superimposed signal x_k expressed by (7). Since the ICA and ambiguities elimination process are the same at FU and NU ends, the subscripts F and N for the equalized signal as shown in Fig. 1 are not included in this subsection.

There exist ambiguities in the ICA equalized signal $\tilde{x}_k$, including phase and quadrant ambiguities, compared with the original superimposed signal x_k, as:

$$\hat{x}_k = e^{j(\chi+\varphi)} \tilde{x}_k, \tag{13}$$

where $\hat{x}_k$ denotes the signal after ambiguity elimination, and χ and φ denote phase ambiguity and quadrant ambiguity, respectively.

Phase Shifting: Due to the drawback of ICA, there exist different phase shifts in the ICA equalized signal $\tilde{x}_k$ compared with the superimposed signal x_k. This can be resolved by phase shifting in the following steps.

Let $e^{j\chi} = b/|b|$ with b denoting the phase shifting factor obtained from the statistical characteristics of $\tilde{x}_k$, calculated as [39]:

$$b = \left\{ \frac{1}{N_{\mathrm{s}}} \sum_{k=1}^{N_{\mathrm{s}}} (\tilde{x}_k)^4 \right\}^{-1/4} e^{j\pi/4}. \tag{14}$$

Quadrant Ambiguity Elimination: The signal after phase shifting still has a quadrant ambiguity, *i.e.*, the phase difference comparing to x_k is $\varphi\left(\varphi \in \left\{0, \frac{\pi}{2}, -\frac{\pi}{2}, \pi\right\}\right)$ due to 4-QAM, which varies from frame to frame. This can be resolved by the assistance of a short pilot.

The pilot symbols are random generated 4-QAM symbols and known at both user ends. Define $s_{\mathrm{pil},k}$ and $\bar{s}_{\mathrm{pil},k}$ as the k-th pilot symbol $(k = 1, 2, ..., N_{\mathrm{pil}})$ and the decoded version after phase shifting with (14). Let $\hat{\varphi}$ denote the estimate of φ, obtained by maximizing the real part of the cross correlation between $s_{\mathrm{pil},k}$ and $\bar{s}_{\mathrm{pil},k}$, *i.e.*,

$$\hat{\varphi} = \arg\max_{\varphi} \Re e\left(\rho\right), \tag{15}$$

where ρ denotes the cross correlation coefficient expressed as [33]

$$\rho = \frac{1}{N_{\mathrm{pil}}} \sum_{k=1}^{N_{\mathrm{pil}}} \left[\left(\bar{s}_{\mathrm{pil},k} e^{j\varphi}\right) s^*_{\mathrm{pil},k}\right]. \tag{16}$$

Since $\sqrt{(1-\alpha)\beta} > \sqrt{(1-\alpha)(1-\beta)}$ always holds, by properly choosing the values of α and β , it can be easily derived

$$e_1 \gg e_2 > 0. \tag{17}$$

Thus, according to (7), $\hat{x}_k$ is directly passed through the decision device to obtain $\hat{s}_{\mathrm{F},k}$, which is the estimate of $s_{\mathrm{F},k}$ at FU end.

C. MLD at NU End

Following the procedure described in Subsection III-B, let $\hat{x}_{\mathrm{N},k}$ denote the estimate of x_k at NU end. Substituting $s_{\mathrm{F},k} = s_{\mathrm{N},k} e^{j\theta_k}$ and $\tilde{s}_{\mathrm{ref},k} = s_{\mathrm{ref}} e^{j\theta^k}$ into (7) yields

$$x_k = \sqrt{P} e^{j\theta_k} \left(e_1 s_{\mathrm{N},k} + e_2 s_{\mathrm{ref},k}\right). \tag{18}$$

Using (18), MLD is exploited to estimate both NU's symbol $s_{\mathrm{N},k}$ and the rotated phase θ_k, according to:

$$\left(\hat{s}_{\mathrm{N},k}, \hat{\theta}_k\right) = \arg\max_{s_{\mathrm{N},k}, \theta_k} \left| \hat{x}_{\mathrm{N},k} - \sqrt{P} e^{j\theta_k} \left(e_1 s_{\mathrm{N},k} + e_2 s_{\mathrm{ref},k}\right) \right|. \tag{19}$$

It is noteworthy that θ_k is a symbol-dependent phase rotation, in addition to the frame-dependent phase rotation in Subsection III-B. Hence, θ_k has to be retrieved with the assistance of the reference data symbol s_{ref}, but cannot be retrieved by the approach presented in Subsection III-B. Without the knowledge of s_{ref} and θ_k at FU end, FU is unable to recover $s_{\mathrm{N},k}$, which enables higher data security of NU.

IV. Performance Analysis and Power Allocation

In this section, we analyze the performance in terms of SER and EE. Based on the derived upper bounds on SER, the optimal precoding constant β and inter-user power allocation coefficient α can be obtained by minimizing the average SER derived.

$$\bar{P}_{e_{\rm ave}} = \frac{7}{4} - \frac{1}{2}\left[\sqrt{\frac{\Gamma\sigma_{h_{\rm F}}{}^2(e_1-e_2)^2}{2+\Gamma\sigma_{h_{\rm F}}{}^2(e_1-e_2)^2}} + \sqrt{\frac{\Gamma\sigma_{h_{\rm F}}{}^2(e_1+e_2)^2}{2+\Gamma\sigma_{h_{\rm F}}{}^2(e_1+e_2)^2}} + \sqrt{\frac{\Gamma\sigma_{h_{\rm N}}{}^2e_2{}^2}{4+\Gamma\sigma_{h_{\rm N}}{}^2e_2{}^2}}\right] - \frac{1}{4}\sqrt{\frac{\Gamma\sigma_{h_{\rm N}}{}^2(e_1-e_2)^2}{4+\Gamma\sigma_{h_{\rm N}}{}^2(e_1-e_2)^2}}. \quad (25)$$

A. SER Performance Analysis

In this subsection, we mainly focus on the ICA output signals assuming perfect ambiguity elimination. Define $\Gamma = P/N_0$ as the transmit signal-to-noise ratio (SNR). Let $\bar{P}_{e_{\rm F}}$ and $\bar{P}_{e_{\rm N}}$ denote the SERs of FU and NU, respectively.

Remark 1: For 4-QAM, FU's closed-form SER is

$$\bar{P}_{e_{\rm F}} = 1 - \frac{1}{2}\left[\sqrt{\frac{\Gamma\sigma_{h_{\rm F}}{}^2(e_1-e_2)^2}{2+\Gamma\sigma_{h_{\rm F}}{}^2(e_1-e_2)^2}} + \sqrt{\frac{\Gamma\sigma_{h_{\rm F}}{}^2(e_1+e_2)^2}{2+\Gamma\sigma_{h_{\rm F}}{}^2(e_1+e_2)^2}}\right], \quad (20)$$

and the asymptotic SER of FU for high SNR is given by

$$\bar{P}_{\rm asym_F} = \frac{1}{2\Gamma\sigma_{h_{\rm F}}{}^2}\left[\frac{1}{(e_1-e_2)^2} + \frac{1}{(e_1+e_2)^2}\right]. \quad (21)$$

Proof: See Appendix A.

Remark 2: The upper bound on NU's SER with 4-QAM is expressed as

$$\bar{P}_{e_{\rm N}} < \frac{3}{4} - \frac{1}{2}\sqrt{\frac{\Gamma\sigma_{h_{\rm N}}{}^2e_2{}^2}{4+\Gamma\sigma_{h_{\rm N}}{}^2e_2{}^2}} - \frac{1}{4}\sqrt{\frac{\Gamma\sigma_{h_{\rm N}}{}^2(e_1-e_2)^2}{4+\Gamma\sigma_{h_{\rm N}}{}^2(e_1-e_2)^2}}, \quad (22)$$

and the upper bound on NU's asymptotic SER is given by

$$\bar{P}_{\rm asym_N} < \frac{1}{\Gamma\sigma_{h_{\rm N}}{}^2}\left[\frac{1}{e_2{}^2} + \frac{1}{2(e_1-e_2)^2}\right]. \quad (23)$$

Proof: See Appendix B.

The average SER between two users can be expressed as

$$\bar{P}_{e_{\rm ave}} = \frac{\bar{P}_{e_{\rm F}} + \bar{P}_{e_{\rm N}}}{2}. \quad (24)$$

Using (20) – (23), *Remark 3* can be derived easily as follows.

Remark 3: The upper bound on the two users' average SER can be obtained as (25). let $m = \sigma_{h_{\rm F}}{}^2/\sigma_{h_{\rm N}}{}^2$ denote the PL ratio of the two users. The upper bound on average asymptotic SER is given by

$$\bar{P}_{\rm asym_{ave}} = \frac{1}{2\Gamma\sigma_{h_{\rm F}}{}^2}\left[\frac{m+1}{2m(e_1-e_2)^2} + \frac{1}{2(e_1+e_2)^2} + \frac{1}{me_2{}^2}\right]. \quad (26)$$

B. Power Allocation and Analysis

Based on the asymptotic SER analysis in Subsection IV-A, an efficient power allocation strategy dependent on statistical CSI only is proposed in this subsection. Substituting (8) and (9) into (26) yields an explicit expression of the average asymptotic SER as a function of α, β and m, given by (27). *Lemma 1* can be deduced from (27) as follows.

Lemma 1: The optimal values of inter-user power allocation coefficient α and NU's precoding constant (intra-user power allocation coefficient) β to minimize the average asymptotic SER are dependent on the PL ratio of the two users only, independent of their instantaneous CSI.

An iterative procedure is presented in Algorithm 1 to find the optimal values of α and β, where α^0 is the initial value of α, $u_{\max}$ is the maximum number of iterations, and $\varepsilon_{\max}$ is the decision threshold. Note that this power allocation scheme requires negligible signaling overhead and much lower complexity, compared to the instantaneous CSI based conventional power allocation approaches for NOMA [11].

Algorithm 1 Iterative inter-user and intra-user power allocation algorithm

1: **Initialize**: Initialize the iteration index $u = 0$, inter-user power allocation coefficient α^0 and relative error $\varepsilon^0 = 1$.
2: Search for an initial precoding constant β^0 to minimize (27) with α^0.
3: Compute $\bar{P}^0_{\rm asym_{ave}}$ with α^0 and β^0 obtained in Step 2 by using (27).
4: **while** $u < u_{\max}$ & $\varepsilon^u > \varepsilon_{\max}$
5: $u = u + 1$.
6: Search for α^u to minimize (27) with β^{u-1}.
7: Search for β^u to minimize (27) with α^u obtained in Step 6.
8: Compute $\bar{P}^u_{\rm asym_{ave}}$ with α^u and β^u by using (27).
9: Compute $\varepsilon^u = \left|\bar{P}^u_{\rm asym_{ave}} - \bar{P}^{u-1}_{\rm asym_{ave}}\right| / \bar{P}^u_{\rm asym_{ave}}$.
10: **end while**

Lemma 2: Equal inter-user power allocation (*i.e.*, $\alpha = 0.5$) can result in a near-optimal average asymptotic SER performance. The corresponding NU's precoding constant β increases from 0.5 to a value close to 1 when the PL ratio m increases from 1 (0 dB) to a very large value.

Proof: See Appendix C.

According to *Lemma 2*, it is preferable to choose an initial value of $\alpha^0 = 0.5$ for Algorithm 1. Simulation results in Section VI verify that a 1D search for β by fixing $\alpha = 0.5$ yields a near-optimal performance, meaning that no iteration is needed for Algorithm 1.

$$\bar{P}_{\mathrm{asym_{ave}}} = \frac{1}{2\Gamma\sigma_{h_{\mathrm{N}}}^2}\left\{\frac{1}{(1-\alpha)(1-\beta)} + \frac{m+1}{2+4\sqrt{(1-\alpha)}\left[\sqrt{\alpha\beta}-\sqrt{\alpha(1-\beta)}-\sqrt{\beta(1-\beta)}\right]}\right.$$
$$\left. + \frac{m}{4+8\sqrt{1-\alpha}\left[\sqrt{\alpha\beta}+\sqrt{\alpha(1-\beta)}+\sqrt{\beta(1-\alpha)(1-\beta)}\right]}\right\}. \tag{27}$$

C. EE Analysis

The EE of the proposed IA-ICA scheme is investigated in this subsection. The EE is defined as [40]

$$\eta = \frac{R_{\mathrm{sum}}}{P + P_{\mathrm{DSP}}}, \tag{28}$$

where R_{sum} is the sum rate of NU and FU, and P_{DSP} is the total digital signal processing (DSP) power at both user ends.

Define the achievable rates of FU and NU as R_{F} and R_{N}, respectively. The sum rate of the two users can be obtained as

$$R_{\mathrm{sum}} = R_{\mathrm{F}} + R_{\mathrm{N}}. \tag{29}$$

The sum rate of the proposed IA-ICA is analyzed in the following. We use subscript $i \in \{\mathrm{F}, \mathrm{N}\}$ to denote FU or NU. The time utilization is defined as the ratio of pilot length to frame length, *i.e.*, $\varpi^{\mathrm{IA-ICA}} = \frac{N_{\mathrm{pil}}}{N_{\mathrm{s}}}\left(0 < \varpi^{\mathrm{IA-ICA}} < 1\right)$. Let $\lambda_i^{\mathrm{IA-ICA}}$ denote the receive SINR at user end. Given the total bandwidth B and a target frame error probability of the user $\epsilon_i^{\mathrm{IA-ICA}}$, the achievable rate of the proposed IA-ICA in the finite block regime can be approximated to [41]

$$R_i^{\mathrm{IA-ICA}} \approx \varpi^{\mathrm{IA-ICA}} B\left[C_i^{\mathrm{IA-ICA}} - \sqrt{\frac{V_i^{\mathrm{IA-ICA}}}{N_{\mathrm{s}}}} Q^{-1}\left(\epsilon_i^{\mathrm{IA-ICA}}\right)\right], \tag{30}$$

where

$$C_i^{\mathrm{IA-ICA}} = \log_2\left(1+\lambda_i^{\mathrm{IA-ICA}}\right) \tag{31}$$

denotes the maximum achievable rate by Shannon's capacity theorem, and

$$V_i^{\mathrm{IA-ICA}} = (\log_2 e)^2 \lambda_i^{\mathrm{IA-ICA}} \frac{2+\lambda_i^{\mathrm{IA-ICA}}}{\left(1+\lambda_i^{\mathrm{IA-ICA}}\right)^2} \tag{32}$$

denotes the fading channel dispersion, respectively. The Q function is given by $Q(a) = \int_a^\infty \frac{1}{\sqrt{2\pi}} e^{-t^2/2} dt$. The receive SINR of FU of the proposed IA-ICA is given by

$$\lambda_{\mathrm{F}}^{\mathrm{IA-ICA}} = \frac{\Gamma\left|h_{\mathrm{F}}\right|^2 {e_1}^2}{\Gamma\left|h_{\mathrm{F}}\right|^2 {e_2}^2 + 1}. \tag{33}$$

Substituting (33) into (31) and (32), and using (30), the achievable rate of FU can be obtained. Similarly, we can obtain $R_{\mathrm{N}}^{\mathrm{IA-ICA}}$ with a given $\lambda_{\mathrm{N}}^{\mathrm{IA-ICA}}$ by substituting the subscript in (30), (31) and (33), where $\lambda_{\mathrm{N}}^{\mathrm{IA-ICA}}$ is expressed as [42]

$$\lambda_{\mathrm{N}}^{\mathrm{IA-ICA}} = \frac{\Gamma|h_{\mathrm{N}}|^2 {e_2}^2}{2}. \tag{34}$$

We also analyze the EE achieved by the SIC scheme [21] for comparison. Let $N_{\mathrm{pil}}^{\mathrm{SIC}}$ denote the pilot length for channel estimation of SIC [21], the time utilization of SIC can be calculated as $\varpi^{\mathrm{SIC}} = \frac{N_{\mathrm{pil}}^{\mathrm{SIC}}}{N_{\mathrm{s}}}\left(0 < \varpi^{\mathrm{SIC}} < 1\right)$. The achievable rate of FU of the SIC scheme [21] in the finite block regime can be approximated to

$$R_i^{\mathrm{SIC}} \approx \varpi^{\mathrm{SIC}} B\left[C_i^{\mathrm{SIC}} - \sqrt{\frac{V_i^{\mathrm{SIC}}}{N_{\mathrm{s}}}} Q^{-1}\left(\epsilon_i^{\mathrm{SIC}}\right)\right]. \tag{35}$$

Similar to the analysis of the proposed IA-ICA, the data rate of FU of the SIC method [21] $R_{\mathrm{F}}^{\mathrm{SIC}}$ can be obtained from $\lambda_{\mathrm{F}}^{\mathrm{SIC}}$, given by

$$\lambda_{\mathrm{F}}^{\mathrm{SIC}} = \frac{\Gamma|h_{\mathrm{F}}|^2\alpha}{\Gamma|h_{\mathrm{F}}|^2(1-\alpha)+1}. \tag{36}$$

Assuming perfect cancellation of FU's signal at NU end, the receive SINR of NU of SIC method [21] is expressed as

$$\lambda_{\mathrm{N}}^{\mathrm{SIC}} = \Gamma|h_{\mathrm{N}}|^2(1-\alpha). \tag{37}$$

Substituting (36) and (37) into (29) – (32), the sum rate of the two users of SIC [21] can be obtained easily.

It is worth noting that the power consumptions of the IA-ICA and SIC [21] algorithms can be regarded to be approximately equal, as the DSP power P_{DSP} in (28) for various signal processing algorithms is approximately the same [40]. Thus, to compare IA-ICA and SIC in terms of EE, we focus on the comparison between their achievable data rates. As derived in Appendix D, given a high transmit SNR Γ and a fixed target frame error rate ϵ for both users, the data rates of IA-ICA and SIC can be approximated by

$$R_{\mathrm{sum}}^{\mathrm{IA-ICA}} > \varpi^{\mathrm{IA-ICA}} B\left[\log_2\gamma_{\mathrm{N}} - 1 - 2Q^{-1}(\epsilon)\sqrt{\frac{2}{N_{\mathrm{s}}}}\right] \tag{38}$$

and

$$R_{\mathrm{sum}}^{\mathrm{SIC}} = \varpi^{\mathrm{SIC}} B\left[\log_2\gamma_{\mathrm{N}} - 2Q^{-1}(\epsilon)\sqrt{\frac{2}{N_{\mathrm{s}}}}\right], \tag{39}$$

respectively, where $\gamma_{\mathrm{N}} = \Gamma|h_{\mathrm{N}}|^2$. It can be easily derived that $R_{\mathrm{sum}}^{\mathrm{IA-ICA}} > R_{\mathrm{sum}}^{\mathrm{SIC}}$ as the former has a much shorter pilot length and a much higher time utilization than the latter. Therefore, the proposed IA-ICA scheme is more energy efficient than SIC [21]. This is verified by the simulation results in Section VI.

V. Complexity Analysis

In this section, we study the computational complexity of the proposed IA-ICA scheme, in terms of the number of complex-valued float point multiplications and additions

TABLE I
ANALYTICAL COMPUTATIONAL COMPLEXITY
($N_{\rm sym}$ – Number of source symbols in a frame, $N_{\rm pil}$ – Number of pilot symbols in a frame, N/A – Not applicable).

Item			Order of Complexity			
			Semi-blind IA-ICA	SIC [21]	OPR [24] + MLD with perfect CSI	JMPO [25] with perfect CSI
Transmitter	Precoding		$N_{\rm sym}$	N/A		
	Phase rotation		$N_{\rm sym}$	N/A	$N_{\rm sym}$	
Signal detection at FU end	ICA (JADE)		$N_{\rm sym}+N_{\rm pil}+2$	N/A		
	Ambiguities elimination	Phase shifting	$N_{\rm sym}+N_{\rm pil}$			
		Quadrant ambiguity elimination	$4N_{\rm pil}$			
	MLD / ZF		N/A	$N_{\rm sym}$	$16N_{\rm sym}$	
Signal detection at NU end	ICA (JADE)		$N_{\rm sym}+N_{\rm pil}+2$	N/A		
	Ambiguities elimination	Phase shifting	$N_{\rm sym}+N_{\rm pil}$			
		Quadrant ambiguity elimination	$4N_{\rm pil}$			
	MLD / ZF		$16N_{\rm sym}$	$2N_{\rm sym}$	$16N_{\rm sym}$	
Total			$22N_{\rm sym}+12N_{\rm pil}+4$	$3N_{\rm sym}$	$33N_{\rm sym}$	

over one frame. As shown in Table I, the computational complexity of the proposed IA-ICA scheme is investigated in three aspects, including precoding, rotation at the transmitter, ICA based detection at both user ends and MLD at NU end. The power allocation algorithm by Algorithm 1 is conducted offline based on statistical CSI only, and requires negligible complexity by fixing $\alpha = 0.5$, as discussed in Subsection IV-B. Hence, its complexity is not included in the tables.

The complexity of JADE was analyzed in [39]. The precoding is a superposition of the transmitted symbols and reference data with a complexity of $N_{\rm sym}$. The complexity of the phase rotation is $N_{\rm sym}$. According to (14), phase shifting is of complexity $N_{\rm sym}+N_{\rm pil}$, and the quadrant ambiguity elimination requires a complexity of $4N_{\rm pil}$. MLD is conducted at NU end to estimate NU's symbol and phase rotation. For 4-QAM, there are 4 possible transmit symbols of NU and 4 possible phase shifts. Hence, the complexity of MLD is $16N_{\rm sym}$.

For comparison, the complexity of SIC [21], the optimization of phase rotation (OPR) [24] and the joint modulation and power optimization (JMPO) in [25] with perfect CSI are also analyzed. Assume the simple zero-forcing (ZF) is employed for SIC [21]. The two approaches in [24] and [25] mainly differ in the criterion of selecting the rotation angle. Since the approach in [24] was dedicated to a channel coding system using SIC and cannot work with equal power allocation, we combine MLD with [24] so it works for any power allocation. In [25], MLD is employed at both user ends with a complexity of $16N_{\rm sym}$ at each end. As $N_{\rm pil}$ is much less than $N_{\rm sym}$, the overall complexity of the proposed semi-blind IA-ICA scheme is much less than that of [24] and [25] with perfect CSI.

We set the number of source symbols in a frame to $N_{\rm sym}$ = 498 and pilot length to $N_{\rm pil}$ = 2, resulting in the frame length $N_{\rm s}$ = 500. The normalized complexity is given in Table II. The computational complexity of the proposed semi-blind IA-ICA is about 7 times to that of SIC [21], mainly due to the high-complexity MLD, while the IA-ICA achieves a reduction of about 33.3% over the approaches in [24] and [25] with perfect CSI. It is noteworthy that SIC [21], OPR [24] and JMPO [25] require additional complexity for channel estimation which is not considered here, and they present a worse SER performance with channel estimation errors.

TABLE II
NORMALIZED COMPUTATIONAL COMPLEXITY
($N_{\rm sym} = 498$, $N_{\rm pil} = 2$)

Approach	Normalized Complexity			
	Transmitter	FU end	NU end	Total
Semi-blind IA-ICA	2	2	18	22
SIC [21]	0	1	2	3
OPR [24] + MLD with perfect CSI	1	16	16	33
JMPO [25] with perfect CSI				

VI. SIMULATION RESULTS

In this section, we use Monte Carlo simulations to demonstrate the effectiveness of the proposed IA-ICA scheme. The conventional SIC [21], the OPR [24] along with MLD and the JMPO scheme [25] with perfect CSI are used as references. We assume a frame length of $N_{\rm s} = 500$ 4-QAM symbols and pilot length $N_{\rm pil} = 2$ for ambiguity elimination, except for Figs. 10 and 11. The total bandwidth is set to $B = 5$ MHz. As demonstrated in [40], each process at user ends of IA-ICA can be implemented by TMS320VC33 DSP with a low power consumption of 200 mW, we set $P_{\rm DSP} = 600$ mW. In Figs. 4,

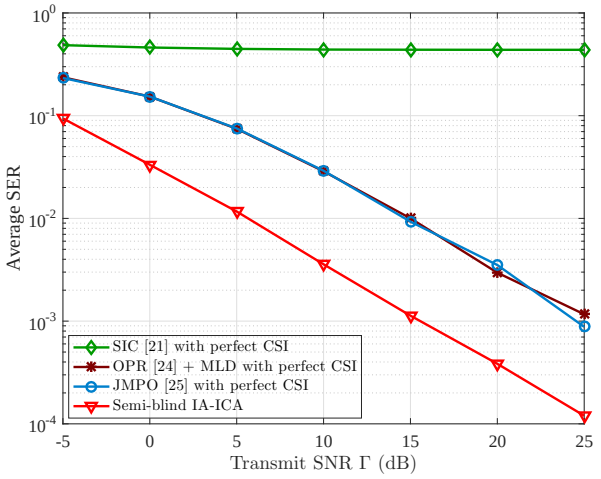

Fig. 4. Average SER performance with PL ratio $m = 20$ dB and inter-user power allocation coefficient $\alpha = 0.5$.

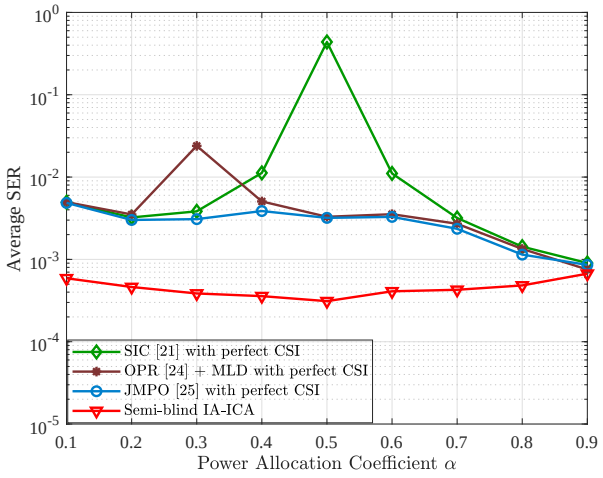

Fig. 5. Impact of power allocation coefficient α on average SER performance with transmit SNR Γ = 20 dB and PL ratio $m = 20$ dB.

6, 9, 10 and 11, equal inter-user power allocation is employed, *i.e.*, the inter-user power allocation coefficient α is set to $\alpha = 0.5$, and the corresponding precoding constant (intra-user power allocation coefficient) β is obtained by Algorithm 1 with only an initial search in Step 2 of Algorithm 1, *i.e.*, no iteration is needed ($u_{\max} = 0$). The decision threshold $\varepsilon_{\max}$ in Algorithm 1 is set to $\varepsilon_{\max} = 10^{-3}$. The channel is assumed to be Rayleigh block fading [25] [43]–[45]. In all simulations, we fix ${\sigma_{h_{\rm F}}}^2/N_0$ at 10 dB, and let ${\sigma_{h_{\rm N}}}^2/N_0$ vary to obtain different values of PL ratio m [25] [46].

Fig. 4 depicts the average SER performance of the two users by the proposed semi-blind IA-ICA structure with equal inter-user power allocation ($\alpha = 0.5$), precoding constant $\beta = 0.85$ and PL ratio $m = 20$ dB. The proposed semi-blind IA-ICA scheme significantly outperforms OPR [24] and JMPO [25] with perfect CSI, presenting an SNR gain of 8 dB at the average SER of 10^{-3}, which perform rotation optimization based on maximizing the smallest Euclidian distance. While the conventional SIC detection approach [21] demonstrates an error floor with equal power allocation. Note that the asymptotic SER based power allocation is effective not only at high SNR, but also in low SNR case.

Fig. 5 demonstrates the impact of the inter-user power allocation coefficient α on average SER performance of the proposed IA-ICA scheme with transmit SNR $\Gamma = 20$ dB and PL ratio m = 20 dB. With a given α, the proposed IA-ICA scheme has a precoding constant β obtained to minimize (27) with no iteration needed. The semi-blind IA-ICA scheme significantly outperforms the other approaches under perfect CSI with a low-to-medium-valued power allocation coefficient as those approaches tend to allocate more power to FU with a worse channel condition. The IA-ICA scheme also demonstrates robustness against inter-user power allocation, with the best SER performance occurring in the case of equal power allocation ($\alpha = 0.5$), while SIC [21] with perfect CSI demonstrates the worst performance at $\alpha = 0.5$. The SER performance of OPR [24] is worst at $\alpha = 0.3$ as the combined effect of phase rotation and the limitation of power allocation

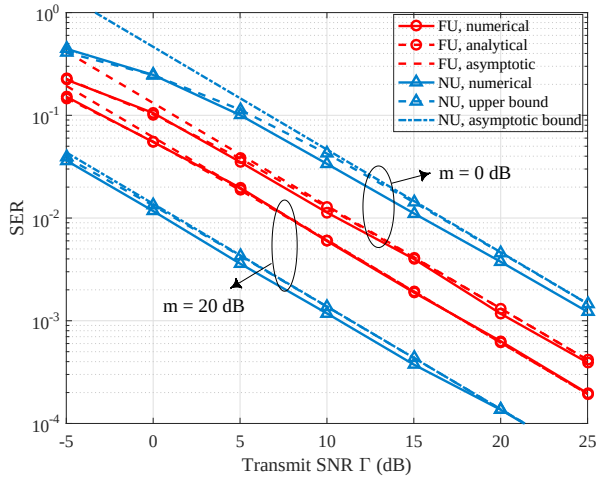

Fig. 6. Analytical and numerical SER performance of FU and NU with the proposed IA-ICA scheme with PL ratio $m = 0$ dB and 20 dB, and inter-user power allocation coefficient $\alpha = 0.5$.

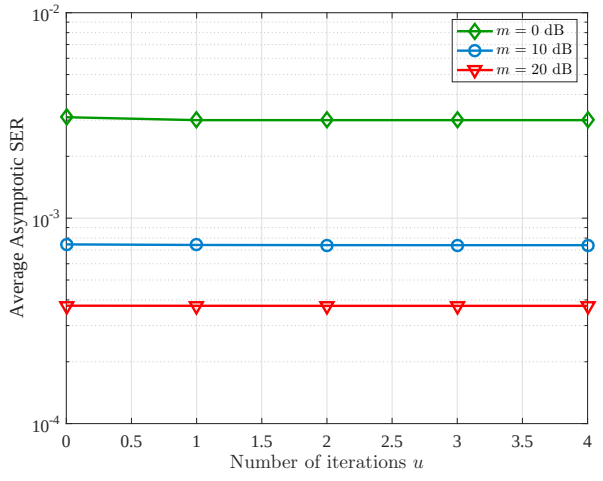

Fig. 7. Convergence behavior of the power allocation algorithm in Algorithm 1 with initial value $\alpha^0 = 0.5$ and transmit SNR Γ = 20 dB.

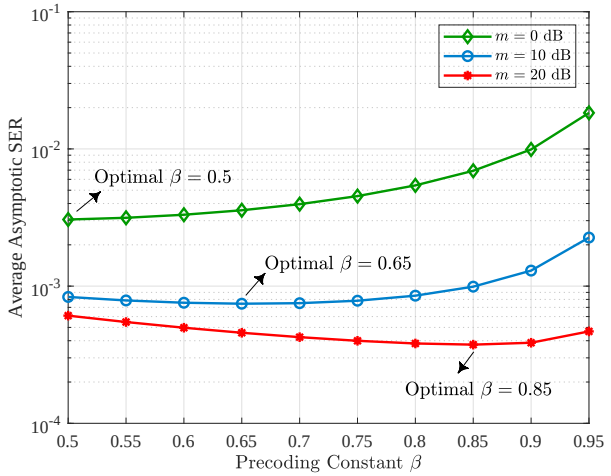

Fig. 8. Impact of precoding constant β on the average asymptotic SER performance with transmit SNR Γ = 20 dB and inter-user power allocation coefficient $\alpha = 0.5$.

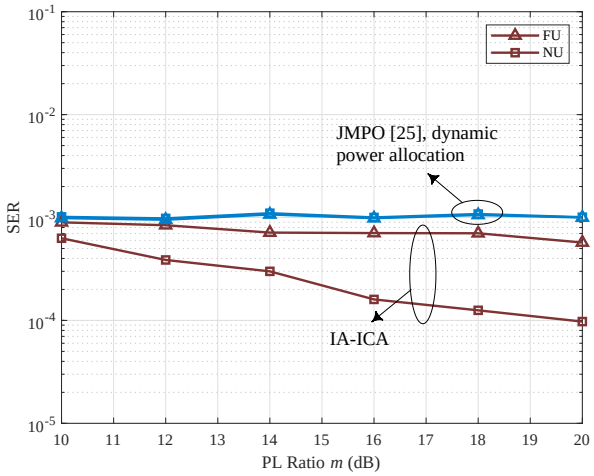

Fig. 9. Impact of PL ratio m on SER at transmit SNR Γ = 20 dB with inter-user power allocation coefficient $\alpha = 0.5$.

by OPR results in a minimum Euclidean distance close to 0, degrading the decoding performance.

In Fig. 6, the numerical SER results are compared with the analytical SER results of FU and NU presented respectively in *Remarks 1* and *2* in Section IV. The value of β is set to $\beta = 0.5$ and 0.85 for $m = 0$ dB and 20 dB, respectively. In both cases, the analytical results are very close to the numerical results. m = 0 dB represents the special case that the distances of two users to BS are the same. In this case, FU achieves a better SER performance than NU, as NU is affected by erroneous detection of the rotated phase. At a large PL ratio of $m = 20$ dB, FU plays a dominant role in the overall SER, as proved in Appendix C.

The convergence behavior of the power allocation algorithm in Algorithm 1 is shown in Fig. 7, with the initial value of $\alpha^0 = 0.5$ and transmit SNR Γ = 20 dB. At various PL ratio values m, the average asymptotic SER by the proposed power allocation algorithm reaches a steady state with no iteration needed, which verifies the efficiency and effectiveness of equal inter-user power allocation, as described in *Lemma 2*.

The impact of precoding constant β on the average asymptotic SER given in (26) is shown in Fig. 8, with inter-user power allocation coefficient $\alpha = 0.5$ and transmit SNR Γ = 20 dB. It can be seen that β plays an important role in minimizing the average asymptotic SER. The optimal value of β increases with the increase of the PL ratio m. It is 0.5 for $m = 0$ dB (*i.e.*, the two users are of equal distance from BS), 0.65 for $m = 10$ dB and 0.85 for $m = 20$ dB, approaching 1 when the PL ratio m gets large. This matches the analysis in *Lemma 2*.

The impact of PL ratio m on FU's and NU's SERs are demonstrated in Fig. 9, where the PL ratio m varies from 10 dB to 20 dB. The performance of the proposed IA-ICA scheme with the values of α and β found by Algorithm 1 is compared to that of JMPO [25] with dynamic power allocation. It can be observed that the proposed IA-ICA approach is superior to JMPO [25] with a higher PL ratio, in terms of SER performance. The performance of JMPO [25] has little change

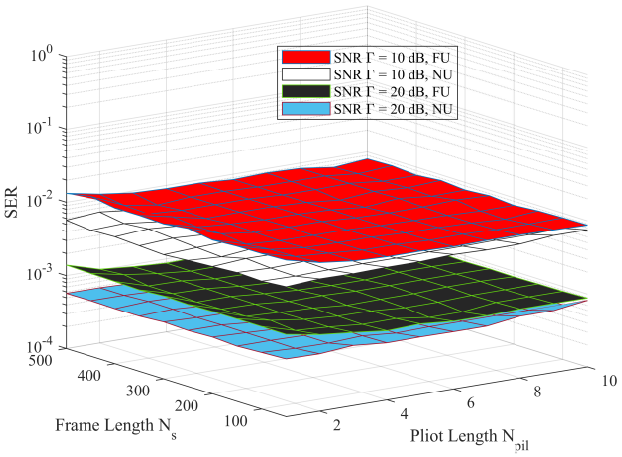

Fig. 10. Impact of frame length and pilot length on SER performance of the proposed IA-ICA approach with PL ratio $m = 10$ dB, inter-user power allocation coefficient $\alpha = 0.5$ and precoding constant $\beta = 0.65$.

over different values of m and the two users provide similar performance.

The impacts of pilot length and frame length on the numerical SER performance of the proposed IA-ICA scheme are shown in Fig. 10, where the transmit SNR is set to Γ = 10 dB and 20 dB, respectively. The pilot length varies from 1 to 10, and the frame length changes from 50 to 500. The SERs of both FU and NU converge with only 1-2 pilot symbols, leading to a training overhead of 0.2-0.4% under a frame length of 500. Also, the average SER is robust against frame length even if it is less than 100. Hence, the proposed system is feasible for HRLL IoT. While larger training overhead is required to implement the approaches in [21], [24] and [25], for channel estimation and CSI feedback.

Fig. 11 shows the EE performance of the proposed IA-ICA with a frame length of $N_s = 100$ and a target error probability $\epsilon = 10^{-4}$, in comparison to SIC [21] with α =

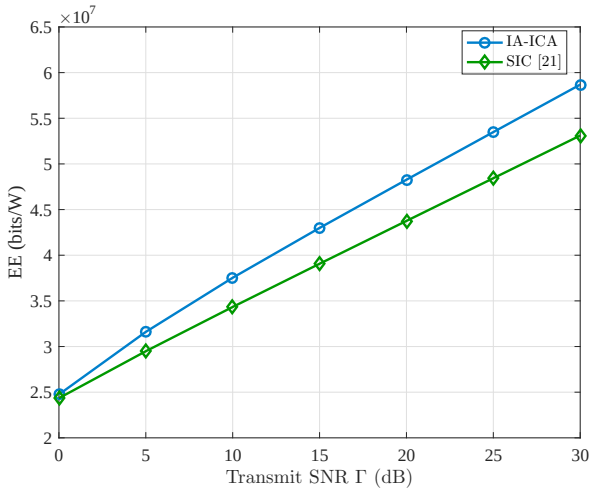

Fig. 11. EE performance of the proposed IA-ICA with PL ratio $m = 20$ dB, frame length $N_{\rm s} = 100$, target error probability $\epsilon = 10^{-4}$, inter-user power allocation coefficient $\alpha = 0.5$, and precoding constant $\beta = 0.85$.

0.7. The time utilization ϖ is assumed to 0.9 [30]. It can been obtained that the proposed IA-ICA approach achieves a higher EE performance than the SIC approach [21], especially at higher SNR. At transmit SNR Γ = 30 dB, the EE performance of the proposed IA-ICA is 11% higher than that of SIC [21].

VII. Conclusion

An IA-ICA based semi-blind structure has been proposed for dual-user downlink NOMA in HRLL IoT. The proposed IA-ICA scheme has very low spectral overhead, with superimposed reference data in non-redundant precoding for phase rotation tracking and only 1-2 pilot symbols for ICA ambiguities elimination, leading to a training overhead of only 0.2-0.4% with a frame length of 500 symbols. It significantly outperforms the conventional SIC based approach [21] and the other phase rotation based approaches [24] [25] for NOMA, even if they are under perfect CSI, as summarized in Table III. Closed-form expressions for the users' SER performance in Rayleigh fading with 4-QAM have been derived, which match the simulation results very well. Based on the analytical results, an efficient power allocation algorithm is proposed, which is dependent on statistical CSI only. The IA-ICA scheme provides a near-optimal performance under equal inter-user power allocation, shown by both analytical and numerical results. Hence, the computational complexity and the signaling overhead involved in power allocation are significantly reduced over the previous work. The SER performance is also robust against a short frame length. Thanks to the reference data unknown to FU, higher physical layer security can be achieved. Hence, the IA-ICA based NOMA system proposed is suitable for HRLL IoT with high reliability, high security, short frame length and low training overhead and negligible signal overhead. This work will be extended to a multi-cell scenario in the future.

Appendix A
Proof of Remark 1

The closed-form expression of FU's SER and its asymptotic form under 4-QAM are derived in this appendix. Let $q^i\,(i = 1, ..., 4)$ denote the i-th symbol on the 4-QAM constellation, as shown in Fig. 3 (a). The union bound on the conditional error probability given that q^i is transmitted is given by [47]

$$p\left(e|q^i\right) \le \sum_{\substack{k=1,\\ k\neq i}}^{4} p_e\left(i,j\right), \tag{40}$$

where $p_e\left(i,j\right)$ denotes the pairwise probability of symbols q^i and q^j. Let d_{ij} denote the distance between the constellation points q^i and q^j. Thus, we have

$$p_e\left(i,j\right) = Q\left(\sqrt{\frac{{d_{ij}}^2}{2N_0}}\right), \tag{41}$$

where the Q function $Q(a)$, represents the probability that a Gaussian variable with zero mean and unit variance is larger than a, and is given by $Q\left(a\right) = \int_a^\infty \frac{1}{\sqrt{2\pi}} e^{-t^2/2} dt$.

We start from the conditional pairwise error probability (PEP). For signal detection at FU end, $s_{{\rm F},k}$ is detected by regarding $e_2\tilde{s}_{{\rm ref},k}$ in (7) as noise. In Fig. 3 (a), the hollow points $\left(q^i, i = 1, ..., 4\right)$ are constellations of $\sqrt{P}e_1 s_{{\rm F},k}$, the solids $\left(x^i, i = 1, ..., 16\right)$ are transmitted symbols $x_k = \sqrt{P}\left(e_1 s_{{\rm F},k} + e_2\tilde{s}_{{\rm ref},k}\right)$. In fact, $\sqrt{P}e_2\tilde{s}_{{\rm ref},k}$ can make a constructive contribution to the detection of $s_{{\rm F},k}$ when x_k is located at the four outer solid points in Fig. 3 (a) $\left(x^i, i = 1, ..., 4\right)$ which is denoted by case A, or destructive contributions when x_k is located at the four inner solid points $\left(x^i, i = 5, ..., 8\right)$ which is denoted by case B. We also consider a case C where x_k is located at the rest eight solid points $\left(x^i, i = 9, ..., 16\right)$ on the constellation shown in Fig. 3 (a). We can derive FU's closed-form SER considering the three possible cases mentioned above. Assuming equally-like transmit symbols, the probabilities of the above three cases are $p\left(A\right) = 1/4, p\left(B\right) = 1/4$ and $p\left(C\right) = 1/2$, respectively.

For case A, the symbol x^i is mistaken for x^j $(i \neq j; i, j = 1, ..., 4)$ when $\left|r_{\rm F} - h_{\rm F}x^i\right|^2 > \left|r_{\rm F} - h_{\rm F}x^j\right|^2$. Thus, the PEP conditioned on $h_{\rm F}$ is calculated as

$$P_{e_{\rm F}}^A\left(x^i \to x^j|h_{\rm F}\right) = Q\left(\sqrt{\frac{\kappa^2}{2N_0}}\right), \tag{42}$$

where $\kappa = \left|h_{\rm F}x^i - h_{\rm F}x^j\right|^2 = 4|h_{\rm F}|^2{d_2}^2$. Using (40) and assuming that errors occurring between the farthest points on the constellation are ignored, the conditional SER for case A can be approximately expressed as

$$P_{e_{\rm F}}^A \approx 2Q\left(\sqrt{\frac{2|h_{\rm F}|^2{d_2}^2}{N_0}}\right). \tag{43}$$

Similarly, for case B, the conditional SER is given by

$$P_{e_{\rm F}}^B \approx 2Q\left(\sqrt{\frac{2|h_{\rm F}|^2{d_1}^2}{N_0}}\right). \tag{44}$$

TABLE III
COMPARISON OF THE PROPOSED IA-ICA AND EXISTING SCHEMES
(N/A – Not applicable).

Item	IA-ICA	SIC [21]	[23]	OPR [24]	JMPO [25]
Reliability	High	Medium	High	Medium	High
Robustness against power allocation	Yes	No	Yes	No	No
Power allocation	Static	Dynamic	N/A	N/A	Dynamic
Computational complexity	Medium	Low	High	High	High
Training overhead	Negligible	High	High	High	High

For case C, the conditional SER can be calculated as

$$P_{e_{\mathrm{F}}}^{C} \approx Q\left(\sqrt{\frac{2|h_{\mathrm{F}}|^2 {d_1}^2}{N_0}}\right) + Q\left(\sqrt{\frac{2|h_{\mathrm{F}}|^2 {d_2}^2}{N_0}}\right). \quad (45)$$

Define $\gamma_{\mathrm{F}} = \Gamma|h_{\mathrm{F}}|^2$ as the receive SNR at FU end given channel gain h_{F}. By the total probability theorem and according to (11) and (12), FU's SER conditioned on h_{F} can be expressed as

$$\begin{aligned} P_{e_{\mathrm{F}}}(\gamma_{\mathrm{F}}) &= \frac{1}{4}P_{e_{\mathrm{F}}}^{A} + \frac{1}{4}P_{e_{\mathrm{F}}}^{B} + \frac{1}{2}P_{e_{\mathrm{F}}}^{C} \\ &\approx Q\left(\sqrt{\gamma_{\mathrm{F}}(e_1-e_2)^2}\right) + Q\left(\sqrt{\gamma_{\mathrm{F}}(e_1+e_2)^2}\right). \end{aligned} \quad (46)$$

In case of Rayleigh fading channel, the averaged SER is computed by averaging the conditional error probability over the fading distribution

$$\bar{P}_{e_{\mathrm{F}}} = \int_0^{\infty} P_{e_{\mathrm{F}}}(\gamma_{\mathrm{F}})\, p(\gamma_{\mathrm{F}}) d\gamma_{\mathrm{F}}, \quad (47)$$

where $p(\gamma_{\mathrm{F}})$ is the probability density function (PDF) of γ_{F} given by [47]

$$p(\gamma_{\mathrm{F}}) = \frac{1}{\Gamma{\sigma_{h_{\mathrm{F}}}}^2} e^{-\gamma_{\mathrm{F}}/\Gamma{\sigma_{h_{\mathrm{F}}}}^2}. \quad (48)$$

Substituting (46) and (48) into (47) and referring to Eq. (6.61) in [47] yields FU's closed-form SER, which is given by (20).

Furthermore, we derive the asymptotic expression of FU's SER at very high transmit SNR Γ. (20) can be rewritten as

$$\begin{aligned} \bar{P}_{e_{\mathrm{F}}} = \frac{1}{2}\left\{1 - \frac{1}{\sqrt{2/\left[\Gamma{\sigma_{h_{\mathrm{F}}}}^2(e_1-e_2)^2\right]+1}}\right\} \\ + \frac{1}{2}\left\{1 - \frac{1}{\sqrt{2/\left[\Gamma{\sigma_{h_{\mathrm{F}}}}^2(e_1+e_2)^2\right]+1}}\right\}. \end{aligned} \quad (49)$$

When $\Gamma \to \infty$, we have $\lim_{\Gamma\to\infty} \frac{2}{\Gamma{\sigma_{h_{\mathrm{F}}}}^2(e_1-e_2)^2} = 0$ and $\lim_{\Gamma\to\infty} \frac{2}{\Gamma{\sigma_{h_{\mathrm{F}}}}^2(e_1+e_2)^2} = 0$. By exploiting $\lim_{x\to 0}(1+x)^{\alpha} = \alpha x + 1$, we can derive the asymptotic SER of FU as

$$\bar{P}_{\mathrm{asym_F}} = \frac{1}{2\Gamma{\sigma_{h_{\mathrm{F}}}}^2}\left[\frac{1}{(e_1-e_2)^2+1} + \frac{1}{(e_1+e_2)^2+1}\right], \quad (50)$$

(50) can be easily reorganized into the expression of (21).

APPENDIX B
PROOF OF REMARK 2

In this appendix, the SER of NU is analyzed. At NU end, MLD is employed according to (19). NU's SER can be expressed as

$$P_{e_{\mathrm{N}}} = p\left(\hat{s}_{\mathrm{N},k} \neq s_{\mathrm{N},k}, \hat{\theta}_k \neq \theta_k\right) + p\left(\hat{s}_{\mathrm{N},k} \neq s_{\mathrm{N},k}, \hat{\theta}_k = \theta_k\right). \quad (51)$$

To simplify the analysis, we substitute $s_{\mathrm{F},k} = s_{\mathrm{N},k}e^{j\theta_k}$ and $\tilde{s}_{\mathrm{ref},k} = s_{\mathrm{ref}}e^{j\theta_k}$ into (19). Thus, MLD is equivalent to signal detection with the composite constellation in Fig. 3 (a). Let $\hat{s}_{\mathrm{FN},k}$ denote the estimate of FU's symbol at NU end and $\hat{s}_{\mathrm{ref},k}$ denote the estimate of $\tilde{s}_{\mathrm{ref},k}$, (51) can be rewritten as

$$\begin{aligned} P_{e_{\mathrm{com}}} &= p\left(\hat{s}_{\mathrm{FN},k} \neq s_{\mathrm{F},k}, \hat{s}_{\mathrm{ref},k} \neq \tilde{s}_{\mathrm{ref},k}\right) \\ &+ p\left(\hat{s}_{\mathrm{FN},k} = s_{\mathrm{F},k}, \hat{s}_{\mathrm{ref},k} \neq \tilde{s}_{\mathrm{ref},k}\right) \\ &+ p\left(\hat{s}_{\mathrm{FN},k} \neq s_{\mathrm{F},k}, \hat{s}_{\mathrm{ref},k} = \tilde{s}_{\mathrm{ref},k}\right), \end{aligned} \quad (52)$$

(52) can also be expressed as

$$\begin{aligned} P_{e_{\mathrm{com}}} = p\left(\hat{s}_{\mathrm{N},k}{=}s_{\mathrm{N},k}, \hat{\theta}_k \neq \theta_k\right) + p\left(\hat{s}_{\mathrm{N},k} \neq s_{\mathrm{N},k}, \hat{\theta}_k \neq \theta_k\right) \\ + p\left(\hat{s}_{\mathrm{N},k} \neq s_{\mathrm{N},k}, \hat{\theta}_k = \theta_k\right). \end{aligned} \quad (53)$$

Thus, $P_{e_{\mathrm{N}}} < P_{e_{\mathrm{com}}}$. We focus on the decomposite constellation in Fig. 3 (b) to simplify the analysis of $P_{e_{\mathrm{com}}}$. Similar to the analysis approach in (42), the error probability $P_{e_{\mathrm{com}}}$ according to Fig. 3 (b) conditioned on h_{N} can be derived as

$$P_{e_{\mathrm{com}}} \approx \frac{1}{2}Q\left(\sqrt{\frac{2|h_{\mathrm{N}}|^2 {d_1}^2}{N_0}}\right) + Q\left(\sqrt{\frac{|h_{\mathrm{N}}|^2(d_2-d_1)^2}{2N_0}}\right). \quad (54)$$

Define the receive SNR at NU end as $\gamma_{\mathrm{N}} = \Gamma|h_{\mathrm{N}}|^2$. Using (11), (12), (54) and $P_{e_{\mathrm{N}}} < P_{e_{\mathrm{com}}}$, NU's SER conditioned on h_{N} is upper bounded by

$$P_{e_{\mathrm{N}}}(\gamma_{\mathrm{N}}) < \frac{1}{2}Q\left(\sqrt{\frac{\gamma_{\mathrm{N}}(e_1-e_2)^2}{2}}\right) + Q\left(\sqrt{\frac{\gamma_{\mathrm{N}}{e_2}^2}{2}}\right). \tag{55}$$

Similar to the analysis of FU's averaged SER in Appendix A, we can obtain the upper bound on NU's averaged SER as shown in (22), and it can also be written as

$$\begin{aligned}\bar{P}_{e_{\mathrm{N}}} < \frac{1}{2}\left[1 - \frac{1}{\sqrt{4/\left(\Gamma{\sigma_{h_{\mathrm{N}}}}^2{e_2}^2\right)+1}}\right] \\ + \frac{1}{4}\left\{1 - \frac{1}{\sqrt{4/\left[\Gamma{\sigma_{h_{\mathrm{N}}}}^2(e_1-e_2)^2\right]+1}}\right\}.\end{aligned} \tag{56}$$

Following the approach to derive the asymptotic SER of FU in Appendix A, the upper bound on NU's asymptotic SER is expressed as

$$\bar{P}_{\mathrm{asym}_{\mathrm{N}}} < \frac{1}{\Gamma{\sigma_{h_{\mathrm{N}}}}^2}\left[\frac{1}{{e_2}^2+2} + \frac{1}{2(e_1-e_2)^2+2}\right], \tag{57}$$

(57) can be written as the form in (23).

Appendix C
Proof of Lemma 2

In this appendix, we prove that equal inter-user power allocation, *i.e.*, $\alpha = 0.5$, enables a near-optimal SER performance with a properly chosen precoding constant (intra-user power allocation coefficient) β for various PL ratio values m.

At very large PL ratio m, FU's asymptotic SER given by (21) plays a dominant role in the average asymptotic SER given by (26), as opposed to NU's asymptotic SER given by (23). Minimizing FU's SER is equivalent to minimizing $d_2 - d_1 = \sqrt{2P}e_2$, the minimum distance between symbols $x^i\,(i = 1, \ldots, 16)$ in Fig. 3 (a), while maximizing the distances between the symbols $q^i\,(i = 1, \ldots, 4)$ in Fig. 3 (a), *i.e.*, maximizing e_1. Thus, we need to maximize $e_1 - e_2$ only. According to (8) and (9), e_1 is monotonically increasing on β and e_2 is monotonically decreasing on β. Therefore, the average asymptotic SER is minimized when β is close to 1. Then it can be easily proved that when β is close to 1, $e_1 - e_2 = \sqrt{\alpha} + \sqrt{(1-\alpha)}\left(\sqrt{\beta} - \sqrt{1-\beta}\right)$ achieves the maximum value at $\alpha = 0.5$, *i.e.*, the optimal SER performance is obtained by equal power allocation between the two users.

In fact, the choice of β should also take into account the need to estimate the rotated phase θ_k at NU end, which is related to the term $\frac{1}{m{e_2}^2}$ in (26). The larger the value of m, the less the impact of NU's SER on the average SER, and the closer the optimal value of β to 1.

Vice versa, the optimal value of β decreases with the decrease of the value of m. In an extreme case where $m = 1$ (0 dB), *i.e.*, the two users are of equal distance from BS, the average asymptotic SER in (26) can be approximated by

$$\tilde{P}_{\mathrm{asym}_{\mathrm{ave}}} = \frac{1}{2\Gamma{\sigma_{h_{\mathrm{F}}}}^2}\left[\frac{1}{(e_1-e_2)^2} + \frac{1}{{e_2}^2}\right]. \tag{58}$$

The derivatives of $\tilde{P}_{\mathrm{asym}_{\mathrm{ave}}}$ in (58) with respect to (w.r.t.) α and β are given by (59) and (60), respectively. It can be easily proved that $\tilde{P}_{\mathrm{asym}_{\mathrm{ave}}}$ in (58) is monotonically increasing on β when $\alpha = 0.5$, with the minimum SER occurring when $\beta = 0.5$, and that $\tilde{P}_{\mathrm{asym}_{\mathrm{ave}}}$ is convex w.r.t. α when $\beta = 0.5$. Thus, a value of α that makes (59) close to 0 is a value that is close to the global optimal solution.

Substituting $\alpha = 0.5$ and $\beta = 0.5$ into (59) yields

$$\left.\frac{\partial\tilde{P}_{\mathrm{asym}_{\mathrm{ave}}}}{\partial\alpha}\right|_{\alpha=0.5,\beta=0.5} = \frac{2}{\Gamma{\sigma_{h_{\mathrm{F}}}}^2}. \tag{61}$$

With a large valued Γ, (61) is close to 0. Hence, $\alpha = 0.5$ and $\beta = 0.5$ is a near-optimal power allocation result at $m = 0$ dB and large transmit SNR.

Appendix D
Proof of (38) and (39)

The sum rate of the two users is given by

$$R_{\mathrm{sum}} = \varpi B\left[C_{\mathrm{F}} + C_{\mathrm{N}} - \left(\sqrt{\frac{V_{\mathrm{FU}}}{N_{\mathrm{s}}}} + \sqrt{\frac{V_{\mathrm{NU}}}{N_{\mathrm{s}}}}\right)Q^{-1}(\varepsilon)\right]. \tag{62}$$

First, we give an analysis of the proposed IA-ICA. At high transmit SNR Γ, (33) can be approximated to $\lambda_{\mathrm{F}}^{\mathrm{IA-ICA}} = \frac{{e_1}^2}{{e_2}^2}$. $V_{\mathrm{F}}^{\mathrm{IA-ICA}}$ and $V_{\mathrm{N}}^{\mathrm{IA-ICA}}$ can be further approximated to

$$V_{\mathrm{F}}^{\mathrm{IA-ICA}} \approx (\log_2 e)^2\left(1 - {e_2}^4\right) \tag{63}$$

and

$$V_{\mathrm{N}}^{\mathrm{IA-ICA}} \approx (\log_2 e)^2, \tag{64}$$

respectively. According to (9), there is $e_2 < 1$. Thus both (63) and (64) can be approximated to 2. Then we focus on the capacity achieved by Shannon's theorem. Based on (31), we can obtain that

$$\begin{aligned}C_{\mathrm{F}}^{\mathrm{IA-ICA}} + C_{\mathrm{N}}^{\mathrm{IA-ICA}} &= \log_2\left(1 + \frac{{e_1}^2}{{e_2}^2}\right) + \log_2\left(\frac{\gamma_{\mathrm{N}}{e_2}^2}{2}\right) \\ &> \log_2(\gamma_{\mathrm{N}} - 1).\end{aligned} \tag{65}$$

Substituting (63), (64), and (65) into (62) yields (38).

The sum rate of the two users in SIC [21] can be obtained similarly. The channel dispersion $V_{\mathrm{F}}^{\mathrm{SIC}}$ and $V_{\mathrm{N}}^{\mathrm{SIC}}$ can also be approximated to 2, which is omitted here. The capacity of SIC [21] achieved by Shannon's theorem is given by

$$C_{\mathrm{F}}^{\mathrm{SIC}} + C_{\mathrm{N}}^{\mathrm{SIC}} = \log_2\left(1 + \frac{\alpha}{1-\alpha}\right) + \log_2\left[\gamma_{\mathrm{N}}(1-\alpha)\right], \tag{66}$$

(66) can be further simplified as $\log_2\gamma_{\mathrm{N}}$. Using (62), $R_{\mathrm{sum}}^{\mathrm{SIC}}$ is calculated, as shown in (39).

References

[1] B. Wang, Y. Sun, S. Li and Q. Cao, "Hierarchical matching with peer effect for low-latency and high-reliable caching in social IoT," *IEEE Internet of Things J.*, vol. 6, no. 1, pp. 1193-1209, Feb. 2019.

[2] Z. Ma, M. Xiao, Y. Xiao, Z. Pang, H. V. Poor and B. Vucetic, "High-reliability and low-latency wireless communication for internet of things: Challenges, fundamentals, and enabling technologies," *IEEE Internet of Things J.*, vol. 6, no. 5, pp. 7946-7970, Oct. 2019.

$$\frac{\partial \tilde{P}_{\mathrm{asym_{ave}}}}{\partial \alpha} = \frac{\sqrt{1-\alpha} - \sqrt{\alpha}\left(\sqrt{\beta} - \sqrt{1-\beta}\right)}{-2\Gamma {\sigma_{h_{\mathrm{F}}}}^2 \sqrt{\alpha\left(1-\alpha\right)}\left[\sqrt{\alpha} + \sqrt{1-\alpha}\left(\sqrt{\beta} - \sqrt{1-\beta}\right)\right]^3} + \frac{1}{2\Gamma {\sigma_{h_{\mathrm{F}}}}^2 (1-\alpha)^2 (1-\beta)}. \tag{59}$$

$$\frac{\partial \tilde{P}_{\mathrm{asym_{ave}}}}{\partial \beta} = \frac{-\sqrt{1-\alpha}\left(\sqrt{\beta} + \sqrt{1-\beta}\right)}{2\Gamma {\sigma_{h_{\mathrm{F}}}}^2 \sqrt{\beta\left(1-\beta\right)}\left[\sqrt{\alpha} + \sqrt{1-\alpha}\left(\sqrt{\beta} - \sqrt{1-\beta}\right)\right]^3} + \frac{1}{2\Gamma {\sigma_{h_{\mathrm{F}}}}^2 \left(1-\alpha\right)\left(1-\beta\right)^2}. \tag{60}$$

[3] G. Liu, Z. Wang, J. Hu, Z. Ding and P. Fan, "Cooperative NOMA broadcasting/multicasting for low-latency and high-reliability 5G cellular V2X communications," *IEEE Internet of Things J.*, vol. 6, no. 5, pp. 7828-7838, Oct. 2019.

[4] Y. Hu, C. Schnelling, M. C. Gursoy and A. Schmeink, "Multi-relay-assisted low-latency high-reliability communications with best single relay selection," *IEEE Trans. Veh. Tech.*, vol. 68, no. 8, pp. 7630-7642, Aug. 2019.

[5] J. Zeng, T. Lv, R. P. Liu, X. Su, Y. J. Guo and N. C. Beaulieu, "Enabling ultra-reliable and low latency communications under shadow fading by massive MU-MIMO," *IEEE Internet of Things J.*, 2019 (early access).

[6] C. She, Y. Duan, G. Zhao, T. Q. S. Quek, Y. Li and B. Vucetic, "Cross-layer design for mission-critical IoT in mobile edge computing systems," *IEEE Internet of Things J.*, 2019 (early access).

[7] Q. Wu, W. Chen, D. W. K. Ng and R. Schober, "Spectral and energy-efficient wireless powered IoT networks: NOMA or TDMA?," *IEEE Trans. Veh. Tech.*, vol. 67, no. 7, pp. 6663-6667, Jul. 2018.

[8] K. Yang, N. Yang, N. Ye, M. Jia, Z. Gao and R. Fan, "Non-orthogonal multiple access: Achieving sustainable future radio access," *IEEE Commun. Mag.*, vol. 57, no. 2, pp. 116-121, Feb. 2019.

[9] Z. Ding et al., "Application of non-orthogonal multiple access in LTE and 5G networks," *IEEE Commun. Mag.*, vol. 55, no. 2, pp. 185-191, Feb. 2017.

[10] B. Di, L. Song, Y. Li and G. Y. Li, "Non-orthogonal multiple access for high-reliable and low-latency V2X communications in 5G systems," *IEEE J. Sel. Areas Commun.*, vol. 35, no. 10, pp. 2383-2397, Oct. 2017.

[11] Z. Ding, X. Lei, G. K. Karagiannidis, R. Schober, J. Yuan and V. K. Bhargava, "A survey on non-orthogonal multiple access for 5G networks: Research challenges and future trends," *IEEE J. Sel. Areas Commun.*, vol. 35, no. 10, pp. 2181-2195, Oct. 2017.

[12] J. Zeng et al., "Achieving ultra-reliable and low latency communications in IoT by FD-SCMA," *IEEE Internet of Things J.*, 2019 (early access).

[13] S. M. R. Islam, N. Avazov, O. A. Dobre and K. Kwak, "Power-domain non-orthogonal multiple access (NOMA) in 5G Systems: Potentials and challenges," *Commun. Surveys Tuts.* , vol. 19, no. 2, pp. 721-742, Secondquarter 2017.

[14] F. Fang, H. Zhang, J. Cheng, S. Roy and V. C. M. Leung, "Joint user scheduling and power allocation optimization for energy-efficient NOMA systems with imperfect CSI," *IEEE J. Sel. Areas Commun.*, vol. 35, no. 12, pp. 2874-2885, Dec. 2017.

[15] Y. Sun, Z. Ding, X. Dai and O. A. Dobre, "On the performance of network NOMA in uplink CoMP systems: A stochastic geometry approach," *IEEE Trans. Wireless Commun.*, vol. 67, no. 7, pp. 5084-5098, Jul. 2019.

[16] X. Liu, Y. Liu, X. Wang and H. Lin, "Highly efficient 3-D resource allocation techniques in 5G for NOMA-enabled massive MIMO and relaying systems," *IEEE J. Sel. Areas Commun.*, vol. 35, no. 12, pp. 2785-2797, Dec. 2017.

[17] L. Chen, L. Ma and Y. Xu, "Proportional fairness-based user pairing and power allocation algorithm for non-orthogonal multiple access system," *IEEE Access*, vol. 7, pp. 19602-19615, Jan. 2019.

[18] X. Sun, S. Yan, N. Yang, Z. Ding, C. Shen and Z. Zhong, "Short-packet downlink transmission with non-orthogonal multiple access," *IEEE Trans. Wireless Commun.*, vol. 17, no. 7, pp. 4550-4564, Jul. 2018.

[19] C. Xiao et al., "Downlink MIMO-NOMA for ultra-reliable low-latency communications," *IEEE J. Sel. Areas Commun.*, vol. 37, no. 4, pp. 780-794, Apr. 2019.

[20] M. Bennis, M. Debbah, and H. V. Poor, "Ultra-reliable and low-latency wireless communication: Tail, risk, and scale," *Proc. IEEE*, vol. 106, no. 10, pp. 1834–1853, Oct. 2018.

[21] L. Zhu, J. Zhang, Z. Xiao, X. Cao and D. O. Wu, "Optimal user pairing for downlink non-orthogonal multiple access (NOMA)," *IEEE Wireless Commun. Lett.*, vol. 8, no. 2, pp. 328-331, Apr. 2019.

[22] Y. Huang, C. Zhang, J. Wang, Y. Jing, L. Yang and X. You, "Signal processing for MIMO-NOMA: Present and future challenges," *IEEE Wireless Commun.*, vol. 25, no. 2, pp. 32-38, Apr. 2018.

[23] M. Chraiti, A. Ghrayeb and C. Assi, "A NOMA scheme for a two-user MISO downlink channel with unknown CSIT," *IEEE Trans. Wireless Commun.*, vol. 17, no. 10, pp. 6775-6789, Oct. 2018.

[24] Y. Chang and K. Fukawa,"Non-orthogonal multiple access with phase rotation employing joint MUD and SIC," in *Proc. IEEE VTC-Spring 2018*, Porto, Portugal, Jun. 2018, pp. 1-5.

[25] B. K. Ng and C. Lam, "Joint power and modulation optimization in two-user non-orthogonal multiple access channels: A minimum error probability approach," *IEEE Trans. Veh. Technol.*, vol. 67, no. 11, pp. 10693-10703, Nov. 2018.

[26] X. Wang, F. Labeau and L. Mei, "Closed-form BER expressions of QPSK constellation for uplink non-orthogonal multiple access," *IEEE Commun. Lett.*, vol. 21, no. 10, pp. 2242-2245, Oct. 2017.

[27] E. C. Cejudo, H. Zhu, and O. Alluhaibi, "On the power allocation and constellation selection in downlink NOMA," *in Proc. IEEE VTC-Fall 2017*, Toronto, Canada, Sep. 2017, pp. 1–5.

[28] J. W. Kim, S. Y. Shin and V. C. M. Leung, "Performance enhancement of downlink NOMA by combination with GSSK," *IEEE Wireless Commun. Lett.*, vol. 7, no. 5, pp. 860-863, Oct. 2018.

[29] F. Fang, J. Cheng and Z. Ding, "Joint energy efficient subchannel and power optimization for a downlink NOMA heterogeneous network," *IEEE Trans. on Veh. Tech.*, vol. 68, no. 2, pp. 1351-1364, Feb. 2019.

[30] M. Mousaei and B. Smida, "Optimizing pilot overhead for ultra-reliable short-packet transmission," in *Proc. IEEE ICC 2017*, Paris, France, May 2017, pp. 1-5.

[31] B. Lee, S. Park, D. J. Love, H. Ji and B. Shim, "Packet structure and receiver design for low latency wireless communications with ultra-short packets," *IEEE Trans. Commun.*, vol. 66, no. 2, pp. 796-807, Feb. 2018.

[32] J.F. Cardoso, "High-order contrasts for independent component analysis," *Neural Computation*, vol. 11, pp. 157-192, 1999.

[33] Y. Jiang, X Zhu, E. Lim, L. Dong and Y. Huang."Low-complexity independent component analysis based semi-blind receiver for wireless multiple-input multiple-output systems," *International Journal of Design, Analysis and Tools for Integrated Circuits and Systems*, vol. 2, no. 2, pp. 91-98, Aug. 2011.

[34] L. Shen, Y. Yao, H. Wang and H. Wang, "ICA based semi-blind decoding method for a multicell multiuser massive MIMO uplink system in rician/rayleigh fading channels," *IEEE Trans. Wireless Commun.*, vol. 16, no. 11, pp. 7501-7511, Nov. 2017.

[35] Y. Li, M. Jiang, Q. Zhang, Q. Li and J. Qin, "Secure beamforming in downlink MISO non-orthogonal multiple access systems," *IEEE Trans. Veh. Technol.*, vol. 66, no. 8, pp. 7563-7567, Aug. 2017.

[36] B. M. ElHalawany and K. Wu, "Physical-layer security of NOMA systems under untrusted users," in *Proc. IEEE GLOBECOM 2018*, Abu Dhabi, United Arab Emirates, Dec. 2018, pp. 1-6.

[37] Y. Yuan, P. Xu, Z. Yang, Z. Ding and Q. Chen, "Joint robust beamforming and power-splitting ratio design in SWIPT-based cooperative NOMA systems with CSI uncertainty," *IEEE Trans. Veh. Technol.*, vol. 68, no. 3, pp. 2386-2400, Mar. 2019.

[38] J. Zhu, J. Wang, Y. Huang, S. He, X. You and L. Yang, "On optimal power allocation for downlink non-orthogonal multiple access systems," *IEEE J. Sel. Areas Commun.*, vol. 35, no. 12, pp. 2744-2757, Dec. 2017.

[39] L. Sarperi, X. Zhu and A. K. Nandi, "Blind OFDM receiver based on independent component analysis for multiple-input multiple-output systems," *IEEE Trans. Wireless Commun.*, vol. 6, no. 11, pp. 4079-4089, Nov. 2007.

[40] H. Duan, X. Zhu, Y. Jiang, Z. Wei and S. Sun, "An adaptive self-interference cancelation/ utilization and ICA assisted semi-blind full-duplex relay system for LLHR IoT," *IEEE Internet of Things J.* (early access).

[41] G. Durisi, T. Koch and P. Popovski, "Toward massive, ultra-reliable, and low-latency wireless communication with short packets," in *Proc. IEEE*, vol. 104, no. 9, pp. 1711-1726, Sep. 2016.
[42] David Tse, Pramod Viswanath, *Fundamentals of Wireless Commun.*, New York, America: Cambridge University Press, 2005.
[43] F. Kara and H. Kaya, "On the error performance of cooperative-NOMA with statistical CSIT," *IEEE Commun. Lett.*, vol. 23, no. 1, pp. 128-131, Jan. 2019.
[44] Y. Zhang, Z. Yang, Y. Feng and S. Yan, "Performance analysis of cooperative relaying systems with power-domain non-orthogonal multiple access," *IEEE Access*, vol. 6, pp. 39839-39848, Jul. 2018.
[45] Y. Gu, H. Chen, Y. Li, and B. Vucetic,"Ultra-reliable short-packet communications: Half-duplex or full-duplex relaying?" *IEEE Wireless Commun. Lett.*, vol. 7, no. 3, pp. 348–351, Jun. 2018.
[46] M. S. Ali, H. Tabassum and E. Hossain, "Dynamic user clustering and power allocation for uplink and downlink non-orthogonal multiple access (NOMA) systems," *IEEE Access*, vol. 4, pp. 6325-6343, Aug. 2016.
[47] A. Goldsmith, *Wireless Commun.*. New York, America: Cambridge University Press, 2005.

Xin Wan received the B.S. degree in Electronics and Information Engineering from the China University of Geosciences, Wuhan, China, in 2018. She is currently working toward the M.S. degree in Communication and Information Systems at the School of Electrical and Information Engineering, Harbin Institute of Technology, Shenzhen, China. Her research interests include channel equalization, interference alignment, non-orthogonal multiple access and blind source separation.

Xu Zhu (S'02-M'03-SM'12) received the B.Eng. degree (Hons.) in Electronics and Information Engineering from the Huazhong University of Science and Technology, Wuhan, China, in 1999, and the Ph.D. degree in Electrical and Electronic Engineering from The Hong Kong University of Science and Technology, Hong Kong, in 2003. She joined the Department of Electrical Engineering and Electronics, University of Liverpool, Liverpool, U.K., in 2003, as an Academic Member, where she is currently a Reader. She is also with the Harbin Institute of Technology, Shenzhen, China. She has more than 190 peer-reviewed publications on communications and signal processing. Her research interests include MIMO, channel estimation and equalization, resource allocation, cooperative communications, green communications etc.. She has acted as a Chair for various international conferences, such as the Vice-Chair of the 2006 and 2008 ICARN International Workshops, the Program Chair of ICSAI 2012, the Symposium Co-Chair of the IEEE ICC 2016, ICC 2019 and Globecom 2021, and the Publicity Chair of the IEEE IUCC 2016. She has served as an Editor for the IEEE Transactions on Wireless Communications and a Guest Editor for several international journals such as Electronics.

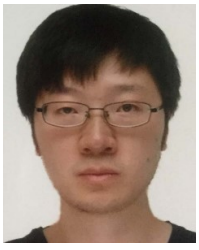

Yufei Jiang (S'12-M'14) received the Ph.D. degree in Electrical Engineering and Electronics from the University of Liverpool, Liverpool, U.K., in 2014. From 2014 to 2015, he was a Postdoctoral Researcher with the Department of Electrical Engineering and Electronics, University of Liverpool. From 2015 to 2017, he was a Research Associate with the Institute for Digital Communications, University of Edinburgh, Edinburgh, U.K. He is currently an Assistant Professor with the Harbin Institute of Technology, Shenzhen, China. His research interests include Li-Fi, synchronization, full-duplex, and blind source separation.

Yujie Liu received the B.Eng. degree in Electrical Engineering and Electronics from the University of Liverpool, Liverpool, U.K., in 2014, and the M.Sc. degree in Communications and Signal Processing from Imperial College London, London, U.K., in 2015. She is currently pursuing the Ph.D. degree with the Department of Electrical Engineering and Electronics, the University of Liverpool, and the Department of Electrical and Electronic Engineering, Xi'an Jiaotong-Liverpool University, Suzhou, China. Her research interests include frequency synchronization, blind channel estimation, full-duplex and 5G new waveforms.

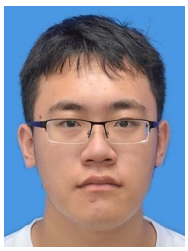

Jiahe Zhao received the B.S. degree in Electronics and Information Engineering from the Harbin Institute of Technology, Harbin, China, in 2018. He is currently working toward the M.S. degree in Communication and Information Systems at the School of Electrical and Information Engineering, Harbin Institute of Technology, Shenzhen, China. His research interests include physical layer security, convex optimization and short-packet communications.